Journal of Molecular Structure 1362 (2026) 145648

Contents lists available at ScienceDirect

Journal of Molecular Structure

journal homepage: www.elsevier.com/locate/molstr

Iono/urothermal synthesis of strontium-MOFs

Michaël Teixeira , Stéphane A. Baudron *

Université de Strasbourg, CNRS, CMC UMR 7140, 4 rue Blaise Pascal, F-67000 Strasbourg, France

ARTICLE INFO

Keywords:
Metal-organic frameworks
Deep eutectic solvents
Ionothermal synthesis
Urothermal synthesis
Strontium
Urea

ABSTRACT

The iono- and urothermal methods, both involving solvents based on e-urea (2-imidazolidinone), the 1:2 choline chloride:e-urea deep eutectic solvent and e-urea hemihydrate respectively, have been explored as synthetic approaches for the preparation of strontium-based metal-organic frameworks (Sr-MOFs). Using these media and seven different di-carboxylic acid ligands, a series of ten Sr-MOFs has been obtained and characterized by X-ray diffraction as well as by thermogravimetric and elemental analyses, infra-red spectroscopy and their optical properties have been investigated. While both preparation methods led to the same unique crystalline phase in some instances, different architectures were obtained for the majority of the ligands explored herein, depending on the synthetic approach employed. This highlights the key role of choline chloride in the ionothermal method and of water in the urothermal strategy, that can act as ligands/templates and thereby impact the formation of intermediate phases and the stability of the materials.

1. Introduction

With their unique properties and features, Metal-Organic Frameworks (MOFs) have attracted much interest over the past three decades [1–5]. These porous crystalline materials have been considered for gas storage/separation, catalysis, biomedicine and drug delivery among others. Fueled by these potential applications in diverse fields, research has also focused on their preparation [6–11]. A variety of synthetic methods have thus been developed and employed, such as microwave-assisted [12], sonochemical [13], mechanochemical [14], electrochemical [15] and solvothermal syntheses [6]. The latter, based on heating, under autogenous pressure, a mixture of ligand and metal source in a solvent has been the most widely explored and applied approach. Common synthetic media for the solvothermal strategy are DMF and DEF, as their decomposition into amines at higher temperature is found to be favorable to the slow deprotonation of the widely used carboxylic acid-based ligands. Alternative solvents have been proposed such as ionic liquids leading to the emergence of ionothermal synthesis [16–20]. More recently, deep eutectic solvents (DESs) [21–25] have also been considered in this context [26,27]. DESs are the combination of compounds at the eutectic ratio affording a mixture showing a strong depression of the melting point in comparison to the one of its individual components and the one expected for the ideal liquid mixture. Their low vapor pressure, relatively wide liquid range, non-flammability and ability to dissolve polar species has made them promising solvents for MOF synthesis. In particular, 1:2 mixtures of choline chloride (ChCl, Fig. 1) and urea derivatives have been employed as solvents for the ionothermal method [26,28–32]. Their decomposition profile [33–34] also generates amines, reminiscent of DMF and DEF, and these DESs have demonstrated their ability to yield a variety of MOFs with interesting textural and/or photophysical properties, to allow the formation of water-sensitive MOFs and to impact the crystalline morphology [26–32]. We have recently focused on the use of the 1:2 ChCl:e-urea DES (e-urea = 2-imidazolidinone, Fig. 1) as solvent for the synthesis of alkaline earth MOFs (AEMOFs) [28–32]. These materials are particularly appealing for the non/low toxicity, and abundance of their metal cations [35–38]. Remarkably, in AEMOFs prepared from this DES, the recurrence of a coordinating motif involving the carbonyl unit assisted by hydrogen bonding of the NH groups of the e-urea from the solvent was observed, whereas ChCl is systematically absent from the crystal structures [30–32]. This shifted our interest to urothermal synthesis, based solely on the use of an urea derivative for the preparation of MOFs. This strategy, albeit less exploited than the ionothermal method, has also demonstrated its capacity to form a diversity of MOFs [39–40]. Surprisingly, to the best of our knowledge, no study has compared the two approaches based on the same urea species to assess the impact of the strategy on the structure and properties of the resulting MOFs.

In this study, a series of seven dicarboxylic acid ligands varying in their length, flexibility and relative position of the coordinating units (Fig. 1) has been employed for the ionothermal and urothermal

* Corresponding author.
E-mail address: sbaudron@unistra.fr (S.A. Baudron).

https://doi.org/10.1016/j.molstruc.2026.145648
Received 10 December 2025; Received in revised form 2 February 2026; Accepted 9 February 2026
Available online 10 February 2026
0022-2860/© 2026 The Authors. Published by Elsevier B.V. This is an open access article under the CC BY license (http://creativecommons.org/licenses/by/4.0/).

preparation of Sr-MOFs in the 1:2 ChCl:e-urea DES and e-urea hemihydrate respectively, aiming to put the two approaches in perspective. The ten resulting MOFs have been characterized by single-crystal and powder X-ray diffraction as well as by thermogravimetric and elemental analyses, infra-red spectroscopy and their optical properties have been investigated.

2. Experimental section

Reagents were obtained from commercial sources and used as received.

General MOF synthesis procedure in the 1:2 ChCl:e-urea DES. The 1:2 ChCl:e-urea DES was prepared before each synthesis by heating a 1:2 mixture of choline chloride and 2-imidazolidinone at 90°C in a round-bottom flask until a homogeneous mixture was formed. The reagents were added to an 8 mL vial before addition of the solvent while hot (90°C) using a preheated syringe. The vial was then heated in a dry bath. After completion of the reaction and before letting the vial cool down, ethanol was added to prevent solidification. The resulting mixture was then filtered and washed multiple times with ethanol. The remaining solid was air-dried.

General MOF synthesis procedure in e-urea hemihydrate. The reagents were added to an 8 mL vial before addition of the solvent. The solvent being solid at ambient temperature (m.p. = 58°C), it was added directly in solid form in the reaction vial. The vial was then heated in a dry bath. After completion of the reaction and before letting the vial cool down, ethanol was added to prevent solidification. The resulting mixture was then filtered and washed multiple times with ethanol. The remaining solid was air-dried. It can be noted that the reaction time under urothermal conditions is generally shorter than under ionothermal conditions to avoid potential evaporation of water at the temperature used that would lead to an increase in the melting point of the reaction medium.

[Sr(3,3'-azo-bpdc)(e-urea)$_2$], Sr-MOF **1**. Urothermal synthesis: Azobenzene-3,3′-dicarboxylic acid (0.0068 g, 0.025 mmol) and Sr(NO$_3$)$_2$ (0.0106 g, 0.05 mmol) were added to an 8 mL vial before addition of solid e-urea hemihydrate (4 g). The vial was then heated at 120°C for 4 days. The reaction was treated according to the general procedure. Ionothermal synthesis: Azobenzene-3,3′-dicarboxylic acid (0.027 g, 0.1 mmol) and Sr(NO$_3$)$_2$ (0.042 g, 0.2 mmol) were added to an 8 mL vial before addition of freshly prepared ChCl:e-urea DES (1:2, 2.5 mL). The vial was then heated at 120°C for 3 weeks. The reaction was treated according to the general procedure (0.0325 g, 61.5 %). Elemental analysis (CHN) for $C_{20}H_{20}N_6O_6Sr$; calculated: C, 45.49; H, 3.82; N, 15.92; found: C, 44.11; H, 4.45; N, 16.43.

[Sr(dpmdc)(e-urea)$_2$], Sr-MOF **2**. Diphenylmethane-4,4′-dicarboxylic acid (0.026 g, 0.1 mmol) and Sr(NO$_3$)$_2$ (0.042 g, 0.2 mmol) were added to an 8 mL before addition of solid e-urea hemihydrate (4 g). The vial was then heated at 120°C for 7 days. The reaction was treated according to the general procedure (0.0272 g, 52.9 %). Elemental analysis (CHN) for $C_{21}H_{22}N_4O_6Sr$; calculated: C, 49.07; H, 4.31; N, 10.90; found: C, 48.65; H, 4.37; N, 10.24.

[Sr(dpmdc)(e-urea)], Sr-MOF **3**. Diphenylmethane-4,4′-dicarboxylic acid (0.026 g, 0.1 mmol) and Sr(NO$_3$)$_2$ (0.042 g, 0.2 mmol) were added to an 8 mL vial before addition of freshly prepared ChCl:e-urea DES (1:2, 2.5 mL). The vial was then heated at 120°C for 2 weeks. The reaction was treated according to the general procedure. To the best of our ability, we were not able to obtain a pure sample of this compound.

[Sr$_2$(bzpdc)$_2$(e-urea)$_3$(H$_2$O)$_2$], Sr-MOF **4**. 4,4′-carbonyldibenzoic acid (0.027 g, 0.1 mmol) and Sr(NO$_3$)$_2$ (0.042 g, 0.2 mmol) were added to an 8 mL vial before addition of solid e-urea hemihydrate (4 g). The vial was then heated at 120°C for 7 days. The reaction was treated

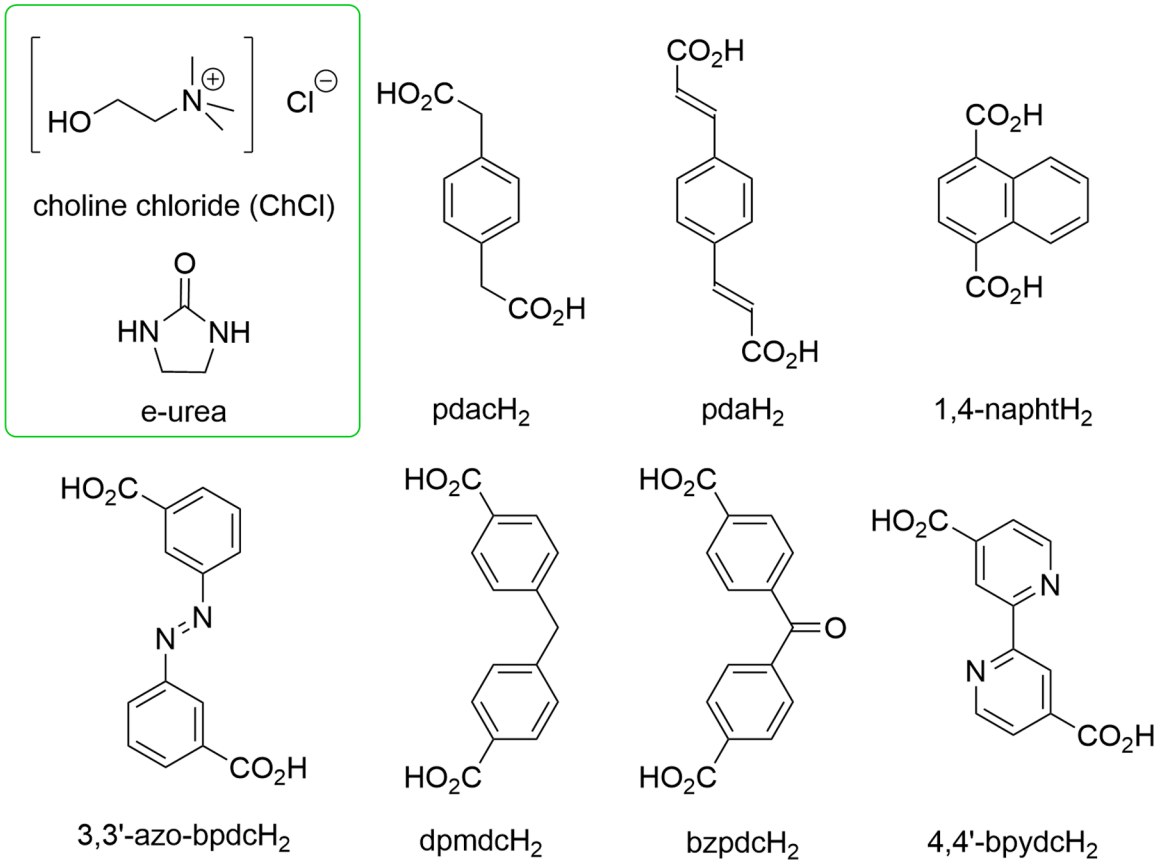

Fig. 1. Representation of the solvent components (green box) and of the seven ligands employed for the preparation of Sr-MOFs via the iono- and urothermal methods.

according to the general procedure (0.0360 g, 71.6 %). Elemental analysis (CHN) for $C_{39}H_{34}N_6O_{13}Sr_2$; calculated: C, 46.56; H, 3.81; N, 8.35; found; C, 46.46; H, 3.88; N, 8.45.

[Sr(4,4'-bpydc)(e-urea)(H_2O)](e-urea), Sr-MOF **5**. 2,2′-bipyridine-4,4′-dicarboxylic acid (0.024 g, 0.1 mmol) and $Sr(NO_3)_2$ (0.042 g, 0.2 mmol) were added to an 8 mL vial before addition of solid e-urea hemihydrate (4 g). The vial was then heated at 120°C for 7 days. The reaction was treated according to the general procedure (0.0253 g, 48.7 %). Elemental analysis (CHN) for $C_{18}H_{20}N_6O_7Sr$; calculated: C, 41.58; H, 3.88; N, 16.16; found; C, 41.03; H, 3.83; N, 16.09.

[Sr(4,4'-bpydc)(e-urea)], Sr-MOF **6**. 2,2′-bipyridine-4,4′-dicarboxylic acid (0.024 g, 0.1 mmol) and $Sr(NO_3)_2$ (0.042 g, 0.2 mmol) were added to an 8 mL vial before addition of freshly prepared ChCl:e-urea DES (1:2, 2.5 mL). The vial was then heated at 120°C for 2 weeks. The reaction was treated according to the general procedure. To the best of our ability, we were not able to obtain a pure sample of the compound.

[Sr(pdac)(e-urea)], Sr-MOF **7**. Ionothermal synthesis: 1,4-Phenylenediacetic acid (0.019 g, 0.1 mmol) and $Sr(NO_3)_2$ (0.042 g, 0.2 mmol) were added to an 8 mL vial before addition of freshly prepared ChCl:e-urea DES (1:2, 2.5 mL). The vial was then heated at 120°C for 10 days. The reaction was treated according to the general procedure. Urothermal synthesis: 1,4-Phenylenediacetic acid (0.019 g, 0.1 mmol) and $Sr(NO_3)_2$ (0.042 g, 0.2 mmol) were added to an 8 mL vial before addition of solid e-urea hemihydrate (4 g). The vial was then heated at 120°C for 2 weeks. The reaction was treated according to the general procedure (0.0172 g, 47.0 %). Elemental analysis (CHN) for $C_{13}H_{14}N_2O_5Sr$; calculated: C, 42.68; H, 3.86; N, 7.66; found: C, 41.52; H, 3.95; N, 8.01.

[Sr(pda)(e-urea)], Sr-MOF **8**. 1,4-Phenylenediacrylic acid (0.022 g, 0.1 mmol) and $Sr(NO_3)_2$ (0.042 g, 0.2 mmol) were added to an 8 mL vial before addition of solid e-urea hemihydrate (4 g). The vial was then heated at 120°C for 7 days. The reaction was treated according to the general procedure (0.0217 g, 44.1 %). Elemental analysis (CHN) for $C_{15}H_{14}N_2O_5Sr$; calculated: C, 46.21; H, 3.62; N, 7.18; found: C, 45.68; H, 3.59; N, 6.91.

[Sr(1,4-napht)(e-urea)$_2$](e-urea), Sr-MOF **9**. 1,4-naphthalenedicarboxylic acid (0.022 g, 0.1 mmol) and $Sr(NO_3)_2$ (0.042 g, 0.2 mmol) were added to an 8 mL vial before addition of solid e-urea hemihydrate (4 g). The vial was then heated at 120°C for 7 days. The reaction was treated according to the general procedure (0.014 g, 25.0 %). Elemental analysis (CHN) for $C_{21}H_{24}N_6O_7Sr$; calculated: C, 45.03; H, 4.32; N, 15.01; found: C, 44.76; H, 4.34; N, 15.04.

[Sr(1,4-napht)(e-urea)], Sr-MOF **10**. 1,4-naphthalenedicarboxylic acid (0.022 g, 0.1 mmol) and $Sr(NO_3)_2$ (0.042 g, 0.2 mmol) were added to an 8 mL vial before addition of freshly prepared ChCl:e-urea DES (1:2, 2.5 mL). The vial was then heated at 120°C for 7 days. The reaction was treated according to the general procedure (0.0263 g, 55.5 % based on [Sr(1,4-napht)(e-urea)$_2$]). Elemental analysis (CHN) for $C_{18}H_{18}N_4O_6Sr$; calculated: C, 45.61; H, 3.83; N, 11.82; found: C, 45.30; H, 3.83; N, 11.26.

2.1. Thermo-gravimetric analysis

The thermal stability of the samples was determined on a PerkinElmer thermogravimetric analyzer TGA 4000 under N_2 flow of 20 mL.min^{-1} and at a heating rate of 5°C.min^{-1} up to 800°C.

2.2. Optical properties

Diffuse reflectance spectra were collected on a PerkinElmer Lambda 650S UV-vis spectrometer at room temperature. Emission spectra were collected on a PerkinElmer LS55 fluorescence spectrometer at room temperature.

2.3. Elemental analysis

Elemental analyses (CHN) were performed at the Service Commun d'Analyses of the University of Strasbourg, in duplicate, employing ThermoFisher FLASH 2000 equipment, whereas the reported values for CHN were taken as the average of two measurements.

2.4. Infrared spectroscopy

Infrared spectra were collected on a PerkinElmer FTIR-UATR Spectrum Two by attenuated total reflectance on powders at room temperature.

2.5. Gas sorption

The textural properties of Sr-MOF **8** were obtained by adsorption-desorption isotherms with N_2 at 77 K in a Micromeritics ASAP 2020 Surface Area and Porosity Analyzer. The Brunauer-Emmett-Teller (BET) method was used for obtaining the specific surface area. A sample of **8**, previously heated at 350°C at a 5°C/min rate aiming at e-urea removal, was outgassed, prior to the N_2 adsorption-desorption analysis, by heating under vacuum at 90°C for 1 h and then at 150°C for 30 minutes and the MicroActive Software version 4.00 was used to analyze the data.

2.6. X-ray diffraction

X-Ray diffraction data collection for **2** and **3** (Table 1) was carried out on a Bruker PHOTON-III DUO CPAD diffractometer equipped with an Oxford Cryosystem liquid N_2 device, using Cu-Kα radiation (λ = 1.54178Å) at 120 K. X-ray diffraction data collection for **1, 4, 5** and **7**-**10** (Tables 1-3) was carried out on a Bruker APEX II DUO Kappa-CCD diffractometer equipped with an Oxford Cryosystem liquid N_2 device, using Mo-Kα radiation (λ = 0.71073 Å) at 173 K. The structures were solved using the program SHELXT-2018 [41]. The refinement and all further calculations were carried out using SHELXL-2018 [42]. The H-atoms were included in calculated positions and treated as riding atoms using SHELXL default parameters. The non-H atoms were refined anisotropically, using weighted full-matrix least-squares on F^2. A semi-empirical absorption correction was applied using SADABS in APEX4 [43]. Note that in the structure of MOFs **3** and **10**, remaining electronic density corresponding to highly disordered solvent molecules that could not be properly refined was treated using the SQUEEZE command [44].

The single-crystal X-ray diffraction data acquisition of **6** (Table 2) was carried out at the CRISTAL beamline (synchrotron SOLEIL, Paris) using the synchrotron radiation source (λ = 0.67199 Å). Diffracted intensities were measured using a CCD detector (Atlas detector from Rigaku) mounted on a four-circles MKS-Newport diffractometer. The crystal-to-detector distance was set to 80 mm. The temperature of the data collection (T = 100 K) was reached with a gas streamer (Cryo-Industries of America). The wavelength was selected with a double crystal monochromator (Si 111 crystals) and sagittal (horizontal) focusing was achieved using a 1D SU-8 compound refractive lenses system developed by the Karlsruhe Institute of Technology. The beam attenuation was performed using Al (or Cu) foils of different thicknesses inserted in the incident beam. Data collection strategies, refinement of the unit cell parameters and the data reduction were carried out using the CrysAlisPro software package [45]. The refinement and all further calculations were carried out using SHELXL-2018 [42].

CCDC 2498769-2498778 contain the supplementary crystallographic data for this paper. These data can be obtained free of charge via http://www.ccdc.cam.ac.uk/conts/retrieving.html

Powder X-ray diffraction patterns were recorded at 293 K on a Bruker D8 diffractometer using monochromatic Cu-Kα radiation with a scanning range between 3 and 40° using a scan step of 1.17° min^{-1}, with the compound placed on a rotating Si low background sample holder. The calculated diagrams were generated with the Mercury® software [46] based on the single-crystal data collected.

Table 1
Crystallographic data for Sr-MOFs **1**-**4**.

	1	**2**	**3**	**4**
Formula	$C_{20}H_{20}N_6O_6Sr$	$C_{21}H_{22}N_4O_6Sr$	$C_{72}H_{64}N_8O_{20}Sr_4$	$C_{39}H_{38}N_6O_{15}Sr_2$
FW	528.04	514.04	1711.79	1005.99
Crystal system	Monoclinic	Monoclinic	Triclinic	Orthorhombic
Space group	$P2_1/n$	$P2_1/n$	P-1	$Pnma$
a, Å	15.9605(14)	13.7781(5)	7.7197(4)	7.2035(8)
b, Å	7.3035(5)	7.2339(3)	22.7419(12)	30.005(4)
c, Å	19.3781(17)	22.8752(8)	23.2985(11)	18.730(3)
α, °			108.701(3)	
β, °	105.104(3)	91.846(3)	90.153(3)	
γ, °			94.490(3)	
V, Å^3	2180.8(3)	2278.77(15)	3860.8(3)	4048.3(10)
Z	4	4	2	4
λ, Å	0.71073	1.54178	1.54178	0.71073
T, K	173(2)	120(2)	120(2)	173(2)
μ, mm^{-1}	2.523	3.672	4.143	2.715
Refls. coll.	26368	28130	111419	52370
Ind. refls. (R_{int})	5230 (0.1214)	4031 (0.1194)	13559 (0.0662)	4766 (0.1667)
R_1 (I>2σ(I))[a]	0.0473	0.0885	0.0710	0.0537
wR_2 (I>2σ(I))[a]	0.0813	0.2282	0.2157	0.1170
R_1 (all data)[a]	0.1000	0.1153	0.0816	0.0975
wR_2 (all data)[a]	0.0969	0.2498	0.2253	0.1388
GOF	0.966	1.065	1.159	1.014

[a] $R_1 = \sum||F_o| - |F_c|\sum/|F_o|$; $wR_2 = [\sum w(F_o^2\text{-}F_c^2)^2/\sum wF_o^4]^{1/2}$

Table 2
Crystallographic data for Sr-MOFs **5**-**8**.

	5	**6**	**7**	**8**
Formula	$C_{18}H_{20}N_6O_7Sr$	$C_{15}H_{12}N_4O_5Sr$	$C_{13}H_{14}N_2O_5Sr$	$C_{30}H_{28}N_4O_{10}Sr_2$
FW	520.02	415.91	365.88	779.80
Crystal system	Monoclinic	Monoclinic	Monoclinic	Triclinic
Space group	$P2_1/n$	$P2_1/c$	$C2/c$	P-1
a, Å	17.119(19)	12.0307(2)	23.144(2)	8.4065(9)
b, Å	7.485(8)	7.45680(10)	13.3692(10)	13.0427(13)
c, Å	17.208(19)	19.7134(2)	8.5119(8)	14.4628(15)
α, °				75.177(4)
β, °	105.431(16)	99.9920(10)	93.847(5)	84.173(4)
γ, °				83.204(5)
V, Å^3	2125(4)	1741.67(4)	2627.8(4)	1518.0(3)
Z	4	4	8	2
λ, Å	0.71073	0.67199	0.71073	0.71073
T, K	173(2)	100 (2)	173(2)	173(2)
μ, mm^{-1}	2.590	2.710	4.128	3.579
Refls. coll.	43821	28104	17746	30174
Ind. refls. (R_{int})	5079 (0.0731)	4946 (0.0594)	3873 (0.1239)	7205 (0.0911)
R_1 (I>2σ(I))[a]	0.0345	0.0330	0.0512	0.0590
wR_2 (I>2σ(I))[a]	0.0741	0.0920	0.1081	0.1208
R_1 (all data)[a]	0.0560	0.0345	0.0988	0.1021
wR_2 (all data)[a]	0.0823	0.0944	0.1305	0.1358
GOF	1.017	1.099	0.995	1.064

[a] $R_1 = \sum||F_o| - |F_c|\sum/|F_o|$; $wR_2 = [\sum w(F_o^2\text{-}F_c^2)^2/\sum wF_o^4]^{1/2}$

Table 3
Crystallographic data for Sr-MOFs **9**-**10**.

	9	**10**
Formula	$C_{21}H_{24}N_6O_7Sr$	$C_{15}H_{12}N_2O_5Sr$
FW	560.08	387.89
Crystal system	Monoclinic	Tetragonal
Space group	$P2_1/n$	$I4_1md$
a, Å	9.0991(7)	23.800(4)
b, Å	15.5143(12)	
c, Å	16.3424(14)	13.078(3)
β, °	97.006(4)	
V, Å^3	2289.8(3)	7408(3)
Z	4	16
λ, Å	0.71073	0.71073
T, K	173(2)	173(2)
μ, mm^{-1}	2.411	2.933
Refls. coll.	15901	41263
Ind. refls. (R_{int})	5456 (0.0627)	4646 (0.2029)
R_1 (I>2σ(I))[a]	0.0387	0.0547
wR_2 (I>2σ(I))[a]	0.0759	0.1181
R_1 (all data)[a]	0.0694	0.1128
wR_2 (all data)[a]	0.0844	0.1441
GOF	1.003	0.968

[a] $R_1 = \sum||F_o| - |F_c|\sum/|F_o|$; $wR_2 = [\sum w(F_o^2\text{-}F_c^2)^2/\sum wF_o^4]^{1/2}$

3. Results and discussion

First, the use of flexible ligands for the synthesis of MOFs was explored under both ionothermal and urothermal conditions in the 1:2 ChCl:e-urea DES and e-urea hemihydrate respectively. Interestingly, in both solvents, Sr-MOF **1** formulated [Sr(3,3'-azo-bpdc)(e-urea)$_2$] (3,3'azo-bpdcH$_2$ = azobenzene-3,3'-dicarboxylic acid) was isolated. It crystallizes in the monoclinic $P2_1/n$ space group with a nine-coordinated Sr(II) cation, bound to two bridging and one chelating carboxylate moieties and four bridging e-urea molecules (Fig. 2). This leads to a 1D secondary building unit (SBU) [47] that, upon bridging by the 3, 3'-azo-bpdc^{2-} ligand, yields a 2D arrangement. This SBU is further stabilized by hydrogen bonding between the e-urea NH groups and neighboring carboxylates. It can be noted that in both solvents systems, Sr-MOF **1** was obtained in pure form as demonstrated by elemental analysis and X-ray powder diffraction, suggesting that, with this ligand, the two synthetic routes yield a unique crystalline system.

An analogous SBU is observed in the crystal structure of Sr-MOF **2** obtained under urothermal conditions with diphenylmethane-4,4′-dicarboxylic acid (dpmdcH$_2$, Fig. 1). This MOF formulated [Sr(dpmdc)(e-urea)$_2$] also crystallizes in the monoclinic $P2_1/n$ space group and shows a 2D arrangement by bridging of the SBU based on a nine-coordinated Sr(II) cation (Fig. 3) with bond distances similar to what is observed in Sr-MOF **1** (Table 4). While the experimental X-ray powder pattern for this material shows the presence of few minor additional peaks (Fig. SM2), no crystal of this potential other side-product could be isolated for further identification. It is worth noting that elemental

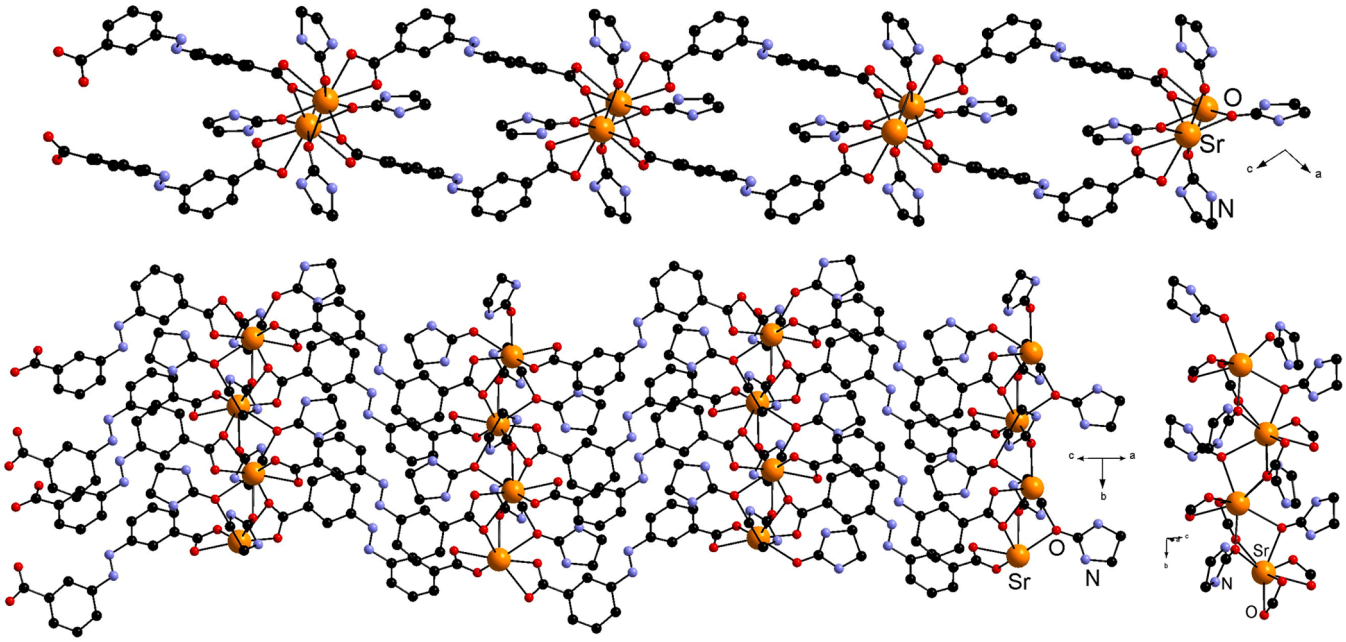

Fig. 2. Side and top views of the 2D arrangement and SBU of the crystal structure of Sr-MOF **1** obtained under both iono- and urothermal conditions. Hydrogen atoms have been omitted for clarity.

analysis for the batch prepared under urothermal conditions was consistent with the Sr-MOF **2** formula, suggesting that this additional phase is minor and/or has the same composition as Sr-MOF **2**. Interestingly, when the reaction was performed in the 1:2 ChCl:e-urea DES, crystals of another phase formulated [Sr(dpmdc)(e-urea)], Sr-MOF **3**, were isolated. Crystallizing in the triclinic *P*-1 space group, it features a 2D arrangement as in Sr-MOFs **1** and **2** but based on two different SBUs comprising eight-coordinated Sr(II) cations, bound to four carboxylate groups and a bridging e-urea molecule (Fig. 3). As for the previous compounds, coordination of the carbonyl unit is assisted by hydrogen bonding between the NH groups and the neighboring carboxylates. The two SBUs differ in the orientation of the urea derivative. X-ray powder diffraction analysis indicated that **3** is not the sole phase forming as additional peaks are observed when compared to the calculated pattern. These peaks however do not correspond to the presence of Sr-MOF **2**, as shown by comparison of the experimental and calculated diffractograms. Furthermore, isolation of single-crystals suitable for X-ray diffraction analysis of potential other phases formed under these conditions could not be performed, preventing characterization of side products. It can be noted that, while there has been one report of another Sr-MOF based on this ligand, [Sr(dpmdc)(H_2O)] [48], the organization and SBUs in **2** and **3** are different and are closer to what is observed for [Mg(dpmdc)$(DEF)_{1/2}$] [48].

Remarkably, when 4,4′-carbonyldibenzoic acid ($bzpdcH_2$, Fig. 1) was used under urothermal conditions in e-urea hemihydrate, another 2D Sr-MOF, **4**, also showing two different SBUs was obtained. Formulated [Sr_2(bzpdc)$_2$(e-urea)$_3$(H_2O)$_2$], it crystallizes in the orthorhombic *Pnma* space group with two independent Sr(II) cations. One is eight-coordinated, bound to four carboxylate units, one bridging water molecule and two terminal e-urea, whereas the other is nine-coordinated, ligated to four carboxylate moieties, a bridging e-urea and a terminal water molecule (Fig. 4). Owing to these varying coordination environments, the distance between consecutive cations is shorter within the SBU based on the eight-coordinated Sr(II) center than within the one based on the nine-coordinated metal center (Table 4).

Sr-MOF **4** was obtained in pure form as demonstrated by X-ray powder diffraction (Fig. SM4) and elemental analysis. It should be noted however that another crystalline phase is formed under ionothermal conditions. However, in spite of our numerous attempts, owing to the small size and limited quality of the crystals, its structure could not be determined.

The presence of water in the solvent in urothermal conditions leads to its incorporation in the SBU as in the case of **4** as well as for **5**, [Sr(4,4'-bpydc)(e-urea)(H_2O)](e-urea) prepared using 2,2′-bipyridine-4,4′-dicarboxylic acid (4,4'-$bpydcH_2$, Fig. 1) in e-urea hemihydrate. In this MOF crystallizing in the monoclinic $P2_1/n$ space group, the Sr(II) cation is nine-coordinated, ligated to four bridging carboxylates and two e-urea molecules as well as one terminal water molecule (Fig. 5). This coordination sphere and the resulting 1D SBU are similar to what is observed in one of the two SBUs in **4**. A solvate e-urea molecule is hydrogen bonded to the coordinated water molecule and carboxylate groups, thereby bridging the 2D sheets. Under ionothermal conditions in the 1:2 ChCl:e-urea DES with the same ligand, the 3D Sr-MOF **6**, [Sr(4,4'-bpydc)(e-urea)], has been obtained. A 1D SBU is formed by bridging of an eight-coordinated Sr(II) bound to four carboxylate and two e-urea molecules (Fig. 5), reminiscent of what has been reported for the Sr-MOF prepared in the same DES with terephtalic acid [32]. This creates rectangular channels occupied by the coordinated e-urea molecules.

For both Sr-MOFs **5** and **6**, the two pyridine units are organized in a *trans* fashion and are not coordinated to a metal cation as described for the Ca-MOF [Ca(4,4'-bpydc)(e-urea)] prepared under ionothermal conditions [31] and unlike what has been reported for Sr-MOFs based on this ligand featuring either coordination to the Sr(II) cation or to another metal center for heterometallic systems [49–51].

It can be noted that no mixture of phases could be detected by X-ray powder diffraction (Figs. SM5-6), suggesting that the nature of the solvent leads to different structures with varying dimensionality, unlike what is observed when performing synthesis with *p*-phenylenediacetic acid ($pdacH_2$, Fig. 1) yielding the same material, Sr-MOF **7** [Sr(pdac)(e-urea)], under both uro-and ionothermal conditions. To the best of our knowledge, this is the first example of a Sr-MOF with this ligand, while a Ca-MOF has been reported [52]. This MOF, crystallizing in the monoclinic *C*2/*c* space group, is based on an eight-coordinated Sr(II) cation, bound to five carboxylates and one terminal e-urea molecule. This leads to the formation of an unusual ladder shaped SBU (Fig. 6). Bridging of this SBU affords a 3D arrangement with channels along the *c* axis occupied by the coordinated e-urea molecules. Remarkably, a similar SBU and overall arrangement is observed in the structure of Sr-MOF **8**,

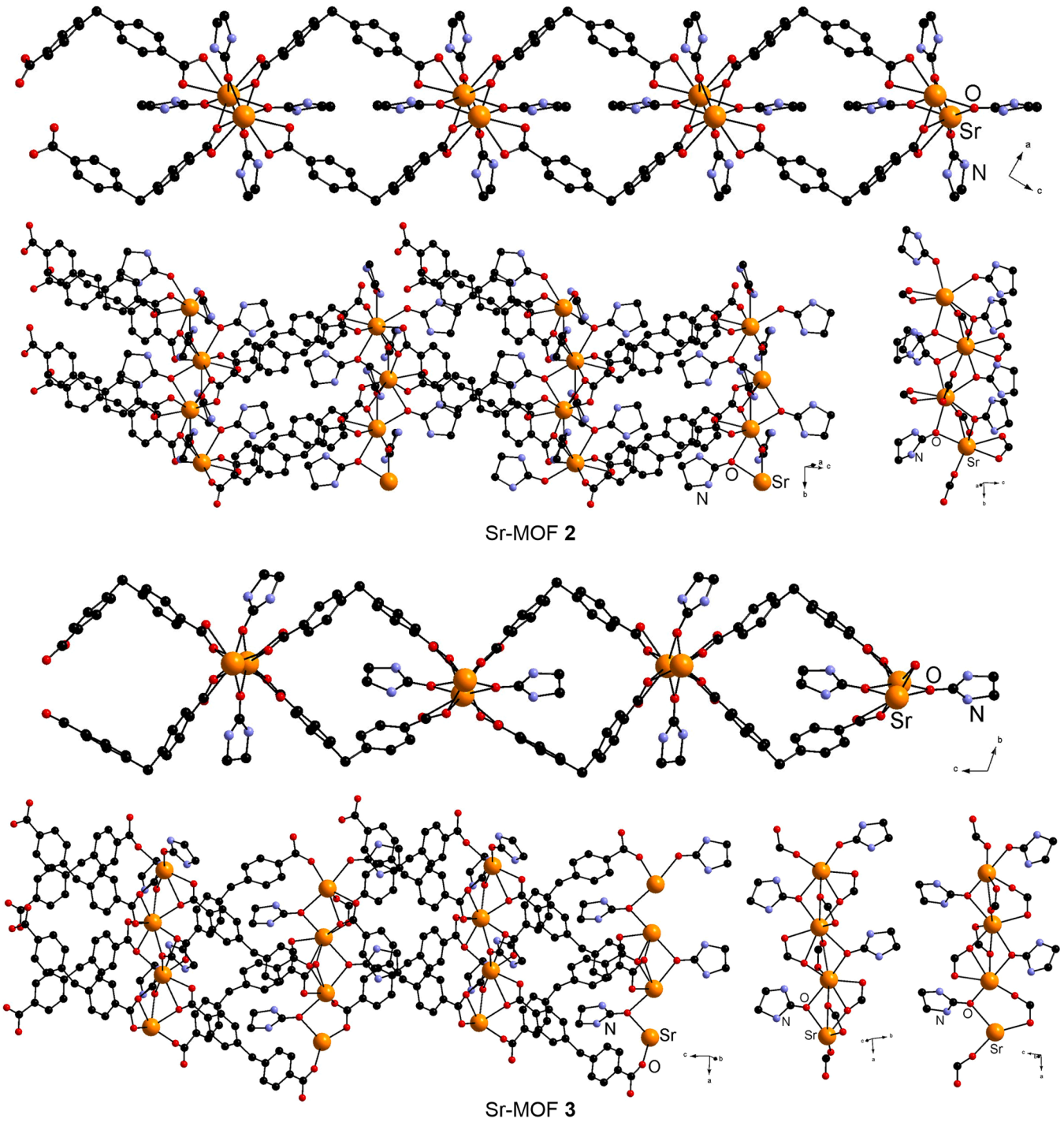

Fig. 3. Side and top views of the 2D arrangement and SBU of the crystal structure of Sr-MOF **2** (top) and **3** (bottom) obtained under uro- and ionothermal conditions, respectively. Hydrogen atoms have been omitted for clarity.

[Sr(pda)(e-urea)], prepared under urothermal conditions using the 1, 4-phenylyenediacrylic acid ($pdaH_2$, Fig. 1). Again, this is the first example of a Sr-MOF prepared with this ligand, while a Ca-MOF prepared under ionothermal conditions has been recently reported [31]. The coordination environment is analogous in **7** and **8** with distances between neighboring Sr(II) cations longer than what is observed for the previous Sr-MOFs where the e-urea is bridging (Table 4). In both MOFs, the e-urea molecules are hydrogen bonded to a carboxylate group on one hand and, in a self-complementary manner, to another e-urea belonging to a SBU across the channels on the other hand. The main difference between the two structures both displaying channels lies in the number of ligands bridging neighboring SBUs. Whereas two $pdac^{2-}$ anions connect the SBUs in **7**, either one or three pda^{2-} act as bridges in **8** (Fig. 6).

The two MOFs could be obtained in pure form as demonstrated by X-ray powder diffraction (Figs SM7-8) and elemental analysis. However, it can be noted that, under ionothermal conditions, ligand $pdaH_2$ led to the formation of another crystalline phase, for which the structure could unfortunately not be determined owing to the poor quality and low diffraction of the material.

Another 3D Sr-MOF was isolated upon reaction of 1,4-naphthalenedicarboxylic acid (1,4-$naphthH_2$, Fig. 1) with $Sr(NO_3)_2$ in e-urea hemihydrate. Sr-MOF **9** formulated [Sr(1,4-napht)(e-urea)$_2$](e-urea),

Table 4
Selected distances (Å) within and between the SBUs and of hydrogen bonds involving the e-urea molecule.

Sr-MOF	Sr-O carboxylate	Sr-O e-urea	Sr-Sr withinSBU	Sr-Sr betweenSBUs	N-H•••O
1	2.553(2)-2.679(2)	2.591(2)-2.663(3)	3.9421(5)	9.8150(8)	2.867(4)-3.148(5)
2	2.528(5)-2.750(7)	2.655(6)-2.683(6)	3.8979(9)	12.320(1)	2.95(1)-3.38(1)
3	2.540(6)-2.711(6)	2.613(6)-2.667(6)	3.938(1)-3.929(1)	11.121(1)	2.77(1)-2.94(1)
4	2.577(3)-2.798(3)	2.536(4)-2.652(4)	3.8773(9)-4.7510(9)	15.055(1)	2.864(5)-2.936(7)
5	2.570(3)-2.796(3)	2.584(3)-2.626(2)	3.992(4)	9.026(7)	2.932(4)-3.124(4)
6	2.590(1)-2.785(1)	2.567(1)-2.629(1)	3.8625(3)	9.6860(5)	2.751(3)-2.859(3)
7	2.496(3)-2.765(3)	2.594(3)	4.1717(7)-4.4503(7)	9.0002(9)	2.851(5)-2.983(5)
8	2.467(5)-2.699(5)	2.578(4)-2.600(4)	4.1769(8)-4.3128(9)	8.823(1)	2.819(8)-2.994(8)
9	2.479(2)-2.569(2)	2.532(2)-2.582(2)	4.0061(5)-5.1720(6)	11.0423(8)	2.826(3)-2.922(4)
10	2.55(1)-2.95(1)	2.592(8)	3.903(3)	8.889(2)	2.89(1)-3.44(1)

crystallizes in the monoclinic $P2_1/n$ space group and is built around a 1D SBU formed around a seven-coordinated Sr(II) cation, bound to four carboxylate moieties and one terminal and two bridging e-urea molecules (Fig. 7). Within the SBU, the bridging and terminal coordinated solvent molecules alternate, yielding distances separating the metal centers varying between a short, 4.006 Å, and a longer one, 5.172 Å (Table 4). As for the other systems, the coordinated e-urea molecules are hydrogen bonded to the carboxylate units. Channels along the *a* axis are formed, occupied by non-coordinated e-urea molecules that are hydrogen bonded in a self-complementary manner. Sr-MOF **9** was isolated in pure form as shown by X-ray diffraction and elemental analysis, demonstrating that the urothermal conditions yielded a unique crystalline phase. When the reaction was performed in the 1:2 ChCl:e-urea DES, Sr-MOF **10**, [Sr(1,4-napht)(e-urea)], was isolated. This 3D-MOF crystallizes in the tetragonal $I4_1md$ space group and features four crystallographically independent Sr(II) cations organized into a helical SBU (Fig. 7). The metal cations are eight-coordinated, ligated to four carboxylates and two bridging e-urea molecules. It is important to note that in the crystal structure there is remaining electronic density suggesting the presence of a highly disordered additional coordinated solvent molecule. This hypothesis is consistent with results from elemental analysis. The quality of the crystallographic data comes from the poor quality of the crystals and the high degree of disorder of this e-urea. The electronic density corresponding to the disordered e-urea molecule was treated using the SQUEEZE command [44]. Unlike other compounds described herein, crystals of Sr-MOF **10** were found to lose their transparency in air over time. However, as demonstrated by X-ray powder diffraction on a sample left in air, this evolution is slow with the material keeping its structure over several days (Fig. SM11). This allowed its complete characterization using a freshly prepared sample.

As previously mentioned, the purity of the different Sr-MOFs described herein has been confirmed by X-ray powder diffraction and elemental analysis. These analyses demonstrated the presence of a single pure crystalline phase, except for Sr-MOF **3** that could not be isolated in pure form (vide supra) and **6** for which only small amounts of the product could be obtained. Furthermore, infra-red spectroscopy demonstrated the absence of remaining unreacted ligand as confirmed in the area between 1500 and 1700 cm^{-1} where the emergence of the $\nu_{as}(COO^-)$ mode of the carboxylate upon coordination to the strontium cation and formation of the MOFs is concomitant with the disappearance of the $\nu(C{=}O)$ stretching mode (Figs SM12-21) [53]. The pure materials were further characterized by thermo-gravimetric analysis (Figs SM30-37). For the 2D Sr-MOFs **1** and **2**, a weight loss corresponding to the mass of solvent molecules is observed over one to three steps. For example, for **2**, two consecutive weight losses amounting to 32 % can be noted between 220 and 360°C matching the expected 33 % of e-urea in the MOF (Fig. SM31). It can be noted that, for **4** incorporating water molecule, the first weight loss starts at a lower temperature (100°C), whereas it starts above 220°C for **1** and **2** (Fig. SM32). A 28 % loss spanning from 100 to 360°C is thus observed, that can be attributed to water and e-urea present in the structure of the material (29 % expected according to the compound formula). Similarly for **5**, a 20 % loss over three steps starting at 120°C may be assigned to the loss of water and e-urea (19.5 % theoretical value). For compounds **7** and **8**, a weight loss

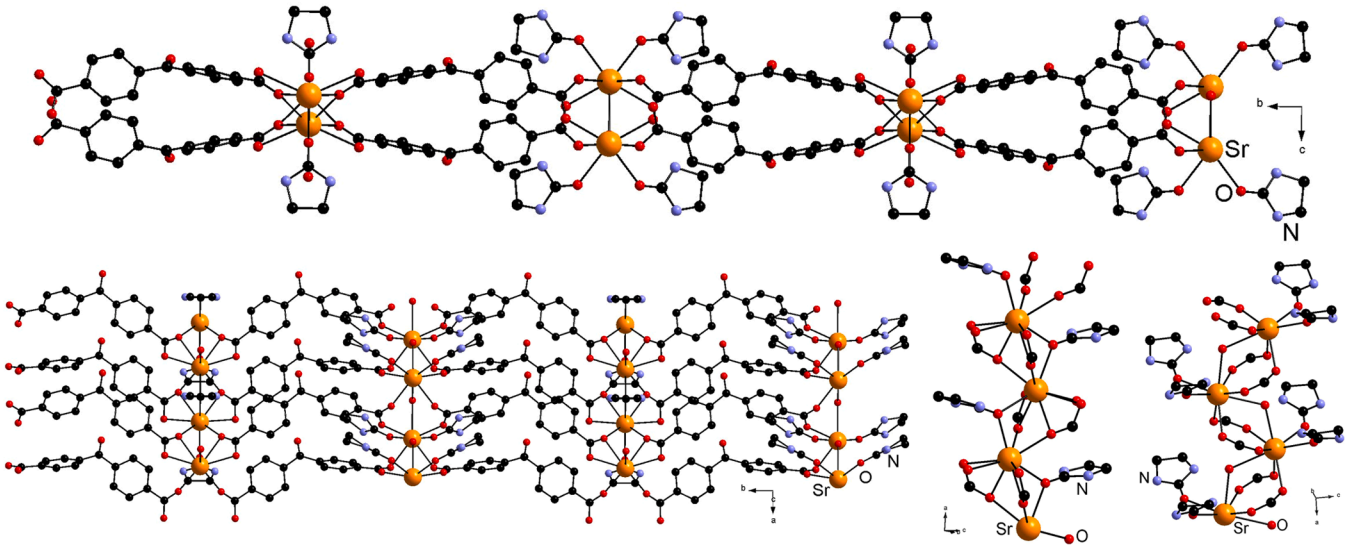

Fig. 4. Side and top views of the 2D arrangement and SBU of the crystal structure of Sr-MOF **4** obtained under urothermal conditions. Note that only one position of the disordered e-urea molecule is shown and that the hydrogen atoms have been omitted for clarity.

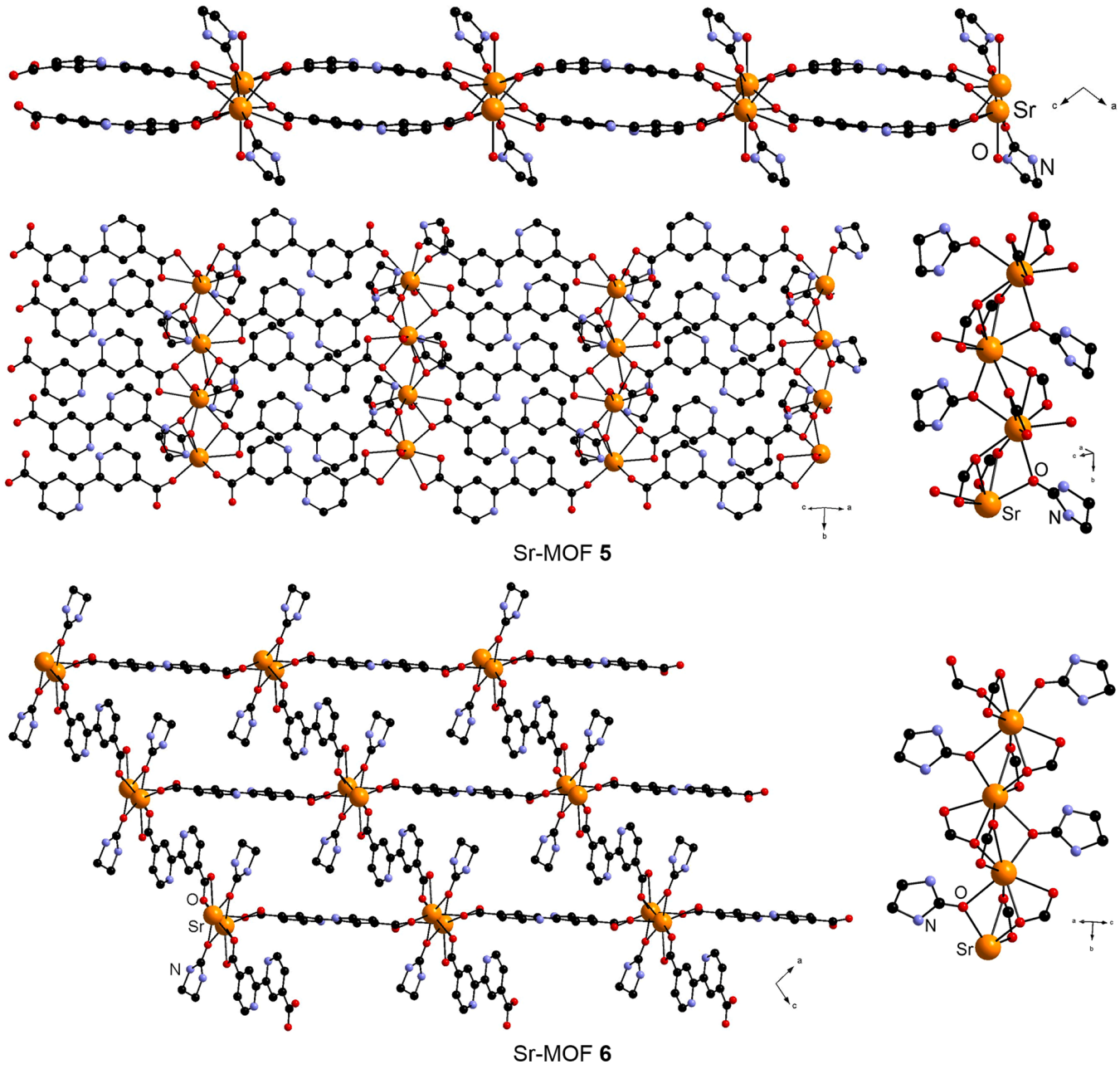

Fig. 5. Side and top views of the 2D arrangement and SBU of the crystal structure of Sr-MOF **5** (top) and 3D arrangement and SBU in **6** (bottom) obtained under uro- and ionothermal conditions, respectively. Hydrogen atoms have been omitted for clarity.

of 21 % starting at 300°C and 20 % at 220°C is observed respectively, corresponding to the percentage of e-urea molecules, 22 and 24 % (Figs. SM34-35). In the case of **8**, the first loss is followed by a plateau. It was thus undertaken to thermally activate the material. In contrast with the 2D Sr-MOFs, this material remained crystalline upon heating at 270°C under N_2 for 45 minutes, as shown by X-ray powder diffraction (Fig. 8). It can however be noted that a broadening of the peaks along with some shift of the peak positions, in particular for peaks at higher 2θ angles, are observed. While this suggests a slight modification of the structure upon heating, the single-crystal structure of the heated sample could unfortunately not be determined. Interestingly, white solid corresponding to sublimated e-urea could be observed following the heating process. Attempts at evacuating the material while heating confirmed the loss of e-urea as demonstrated by a reduction of the presence of nitrogen in elemental analysis. However, study by N_2 sorption-desorption isotherm at 77K unfortunately indicated the absence of porosity for this sample, as the specific surface area calculated by the Brunauer–Emmett–Teller (BET) did not exceed 47.1 $m^2.g^{-1}$. This is substantially lower than 599.5 $m^2.g^-1$ calculated using the pore analyzer module of the MERCURY software [46] for a fully desolvated material. This observation is consistent with a potential modification of the architecture upon e-urea loss. For Sr-MOFs **9** and **10**, activation towards study of their porosity was not further explored given the above-mentioned loss of transparency in air of **10** and the observation that, for **9**, a gradual loss of 50 % weight between 200 and 300°C leads to decomposition of the material (Fig. SM36-37).

The diffuse reflectance spectra of the Sr-MOFs showed the presence of a broad absorption band assigned to intra-ligand transitions (Figs SM22-29). It can be in particular noted that, for **1** incorporating the colored 3,3'-azo-bpdcH^{2-}ligand, absorption extending beyond 500 nm is observed, whereas for the other compounds absorption is detected up to 300 nm for **2** and **7**, and up to 400 nm for **4, 5, 8** and **9**. These

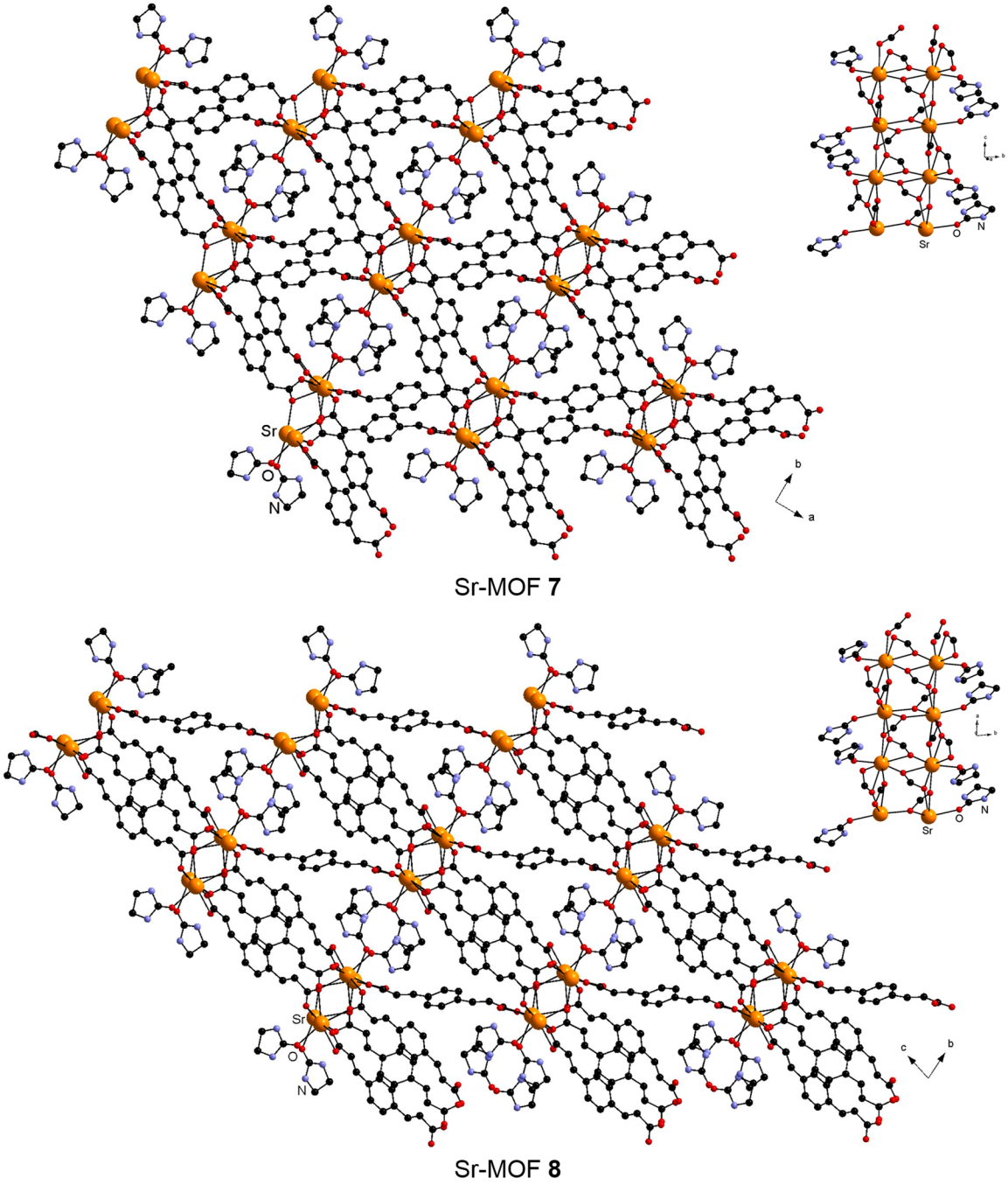

Fig. 6. View along the *c* axis of the 3D arrangement and SBU of the crystal structure of Sr-MOF **7** (top) and **8** (bottom). Hydrogen atoms have been omitted for clarity.

observations are consistent with the spectra reported for Ca-MOFs prepared under ionothermal conditions with the 3,3'-azo-bpdcH_2, pdaH_2, 4,4'-bpydcH_2 and naphtH_2 ligands [31]. The luminescence of the Sr-MOFs was investigated and detectable emission was observed only for Sr-MOFs **9** and **10** incorporating the naphthalene-based ligand. Upon excitation at 290 or 320 nm, a broad emission band centered at 384 and 380 nm for **9** and **10** respectively was observed (Fig. 9). It is blue-shifted when compared to the emission of the free naphtH_2 ligand in the solid state, centered at 496 nm upon excitation at 320 nm. This is consistent with what has been observed for the analogue, [Ca(1,4-napht)(e-urea)], prepared under ionothermal conditions [31] and other reported Sr-, Ca-, Zn- and Cd-MOFs based on this ligand prepared under solvothermal conditions [54–58]. While coordination by Sr(II) may play a role, such blue-shift of ligand-centered emission has been shown to arise from the fact that incorporation of emissive linkers leads to an isolation of the ligand, thereby paralleling luminescence in solution. Hence, formation of the MOFs hinders the red-shift expected when comparing the luminescence of a pure ligand in solution with the one in the solid state [59]. This hypothesis is supported by the report of a Ca-MOF based on napht^{2-} featuring a blue-shifted emission at 395 nm upon excitation at 350 nm, in line with the emission at 412 nm upon excitation at 369 nm of naphtH_2 in a water/ethanol mixed solution (naphtH_2 : water : ethanol = 1 : 1000 : 1000) [56].

4. Conclusion and outlook

In this work, two approaches for the preparation of Sr-MOFs have been explored, the iono- and urothermal methods, both involving

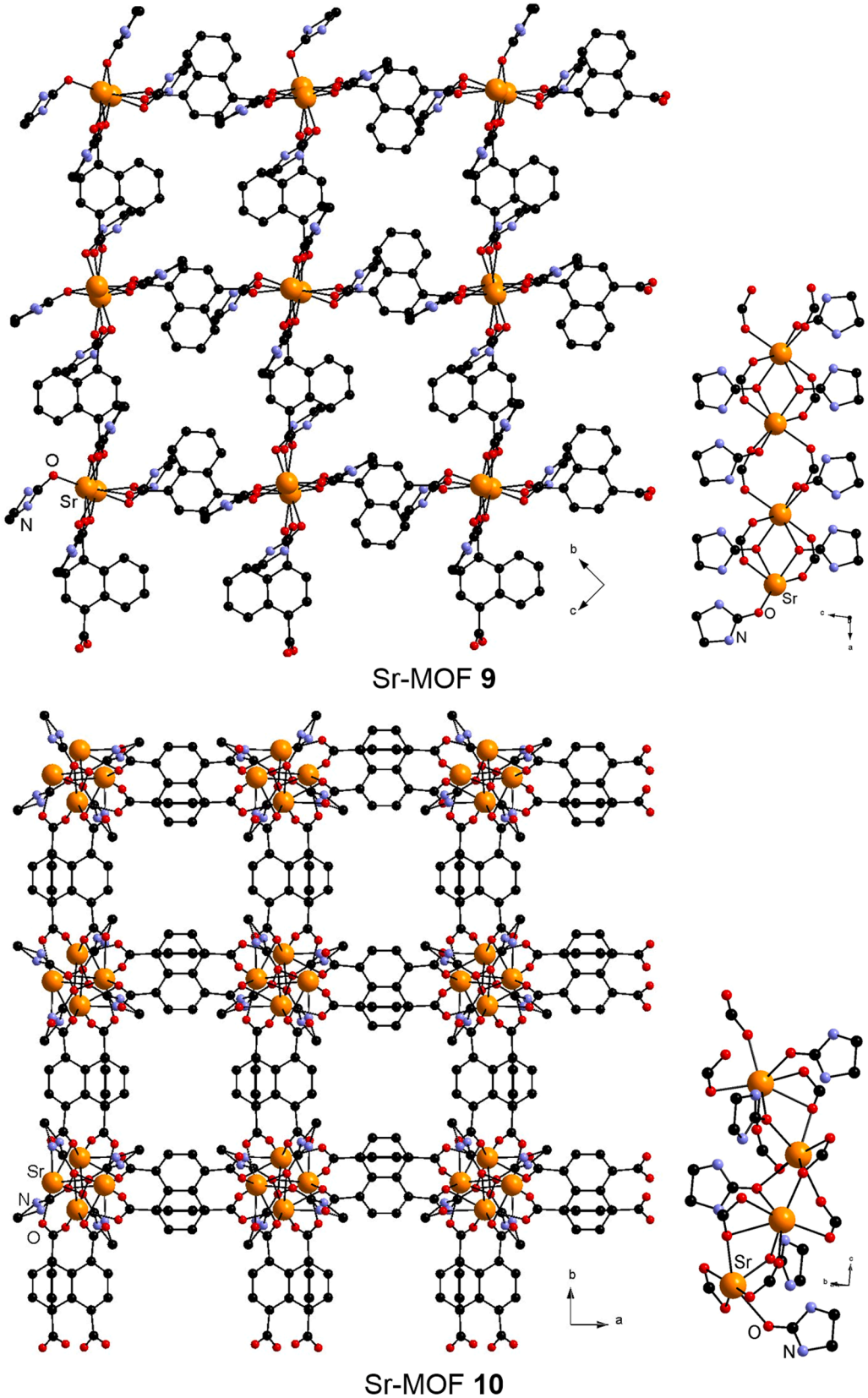

Fig. 7. View of the 3D arrangement and SBU of the crystal structure of Sr-MOF **9** (top) and **10** (bottom). Hydrogen atoms and non-coordinated e-urea molecules have been omitted for clarity.

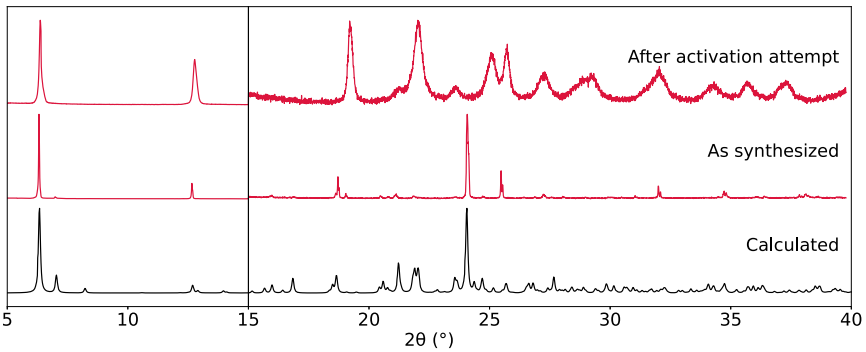

Fig. 8. Comparison of the calculated powder X-ray diffraction patterns of Sr-MOF **8** with the ones obtained experimentally for the as-synthesized compound and for the material heated at 270°C under N_2 for 45 minutes. The intensities have been magnified for 2θ angles above 15° for more clarity and enhanced comparison.

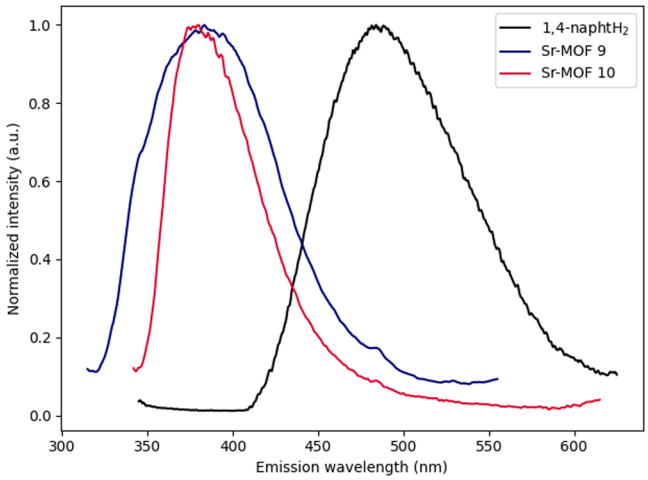

Fig. 9. Solid state emission spectra of ligand naphthH_2 (λ_{ex} = 320 nm) and Sr-MOFs **9** (λ_{ex} = 290 nm) and **10** (λ_{ex} = 320 nm) at room temperature.

solvents based on e-urea, 1:2 ChCl:e-urea DES and e-urea hemihydrate respectively. These synthetic media have been explored with seven different ligands yielding a series of ten materials that were structurally characterized by X-ray diffraction. The two routes were found to be efficient with some similarities and differences. Indeed, in few cases such as for Sr-MOFs **1** and **7**, both approaches led to the same unique crystalline phase. This observation tends to suggest that, in these cases, the presence of ChCl in the DES is not central to the formation of these phases. However, one should note that, for the majority of the ligands explored herein, the two methods afforded different architectures. Two factors may be at stake when comparing the urothermal approach to the ionothermal method. Indeed, e-urea hemihydrate does not incorporate ChCl, unlike the DES, and is composed for one third of water. This latter aspect is particularly relevant for Sr-MOF **5**, prepared under urothermal conditions and incorporating water as ligand, unlike its counterpart prepared in the DES, **6**. Water coordination can nonetheless not be considered as the sole factor, given that ligands 3,3'-azobpdcH_2, dpmdcH_2, pdaH_2 and 1,4-naphthH_2 afforded different MOFs depending on the synthetic approach, with none of them incorporating H_2O. It is most likely a combination of both factors, the presence/absence of ChCl/water, that should be envisaged when trying to rationalize the varying structural outcomes depending on the solvent. As described in a previous report on the synthesis of Mg-MOF 74 in the 1:2 ChCl:e-urea DES [29], the solvent components can act as ligand competitors and form intermediate complexes and polymers involving coordination of e-urea and chloride anions. The formation of these intermediate phases can drive the formation kinetics, morphology and properties of the final MOF. Similarly, while water may not be included in the isolated materials, it can also coordinate giving access to intermediates varying with the ones formed in the DES and thereby leading to different architectures. Furthermore, given the known water-sensitivity of some AEMOFs, some crystalline systems may be unstable in the e-urea hemihydrate driving their disappearance in favor of other more stable systems. Hence rather than opposing the two methods, one should consider exploring both of them for the formation of AEMOFs, as it provides a broader landscape of structures, as demonstrated in this study. In this respect, it is interesting to note the diversity of SBUs characterized in the Sr-MOFs presented herein (Fig. 10). While they differ from SBUs previously observed in Ca- and Sr-MOFs prepared under ionothermal conditions [29–32], a common feature is the predominance of e-urea bridging coordination with only Sr-MOFs **7** and **8** showing terminal e-urea molecules. In all cases, coordination of the solvent molecule is assisted by hydrogen bonding of the NH groups with neighboring carboxylates (Fig. 10).

It would thus be of interest to explore the possibility to form MOFs using fully alkylated urea derivatives. Since these do not form DES with ChCl [21], the ionothermal approach cannot be considered. However, the low meting point of such alkylated urea species opens the door to the exploration of the urothermal strategy for AEMOF preparation. This approach is currently being investigated in our laboratory to further explore the potential of this synthetic approach and will be published in due course.

Accession codes

Deposition Numbers 2498769-2498778 contain the supplementary crystallographic data for this paper. These data can be obtained free of charge via the joint Cambridge Crystallographic Data Centre (CCDC).

Acknowledgements

We thank the Université de Strasbourg, the C.N.R.S., and the Ministère de l'Enseignement Supérieur, de la Recherche et de l'Innovation for financial support. This work was supported by the Interdisciplinary Thematic Institute SysChem, via the IdEx Unistra (ANR-10-IDEX-0002) and by the CSC Graduate School (CSC-IGS ANR-17-EURE-0016) within the French Investments for the Future Program. We acknowledge SOLEIL for provision of synchrotron radiation facilities and we would like to thank Dr. Pierre Fertey for assistance in using beamline CRISTAL (BAG 20231465). We thank Corinne Bailly and Nathalie Gruber (Service de radiocristallographie de la Fédération de Chimie Le Bel – UAR 2042, University of Strasbourg) for assistance in the crystal structure determination.

CRediT authorship contribution statement

Michaël Teixeira: Writing – review & editing, Methodology,

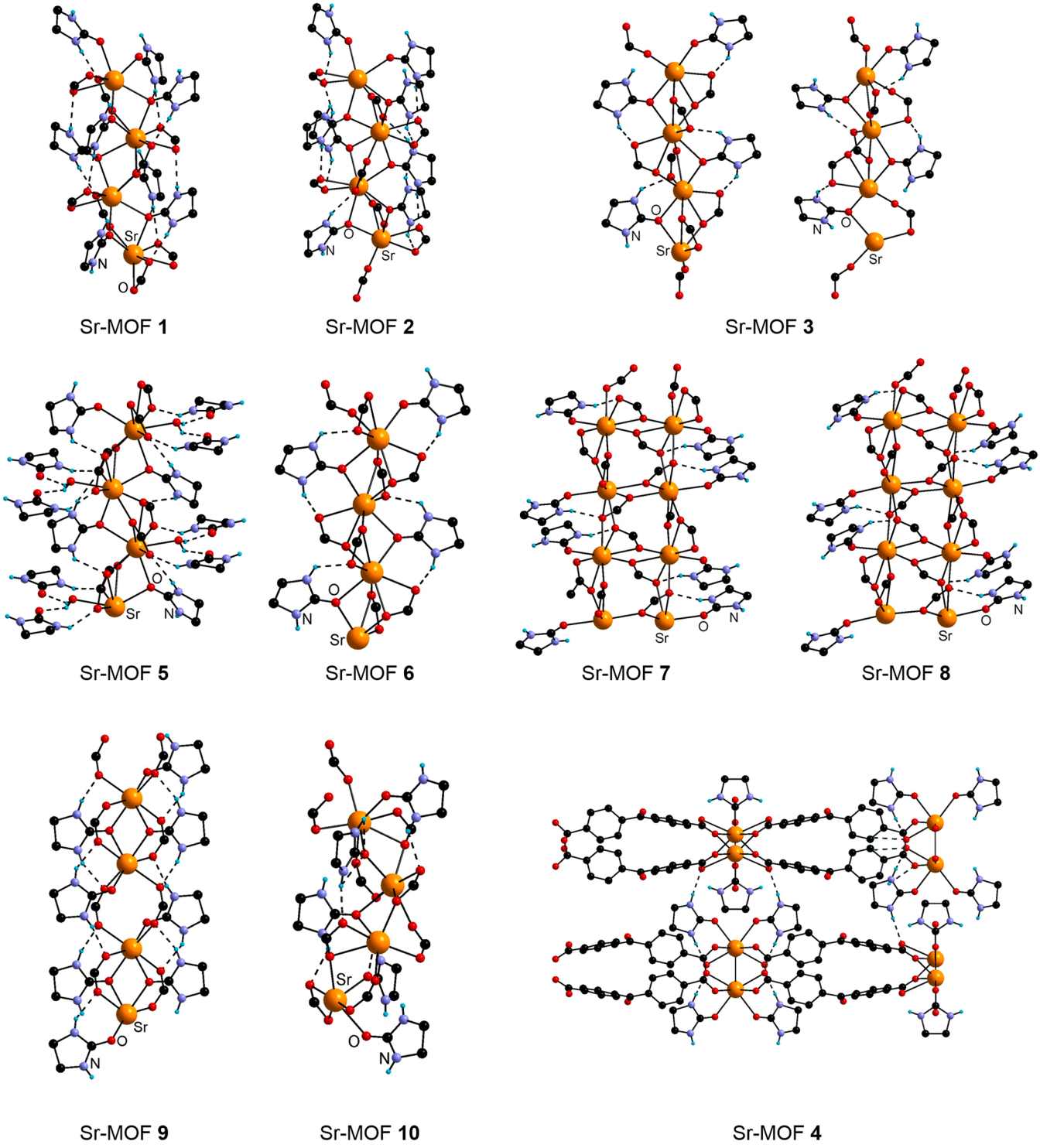

Fig. 10. Representation of the SBUs highlighting the hydrogen bonding networks in Sr-MOFs **1**-**10**.

Investigation. **Stéphane A. Baudron:** Writing – review & editing, Writing – original draft, Supervision, Methodology, Investigation, Funding acquisition, Conceptualization.

Declaration of competing interest

The authors declare that they have no known competing financial interests or personal relationships that could have appeared to influence the work reported in this paper.

Supplementary materials

Supplementary material associated with this article can be found, in the online version, at doi:10.1016/j.molstruc.2026.145648.

Data availability

Data will be made available on request.

References

[1] H.C. Zhou, J.R. Long, O.M. Yaghi, Introduction to Metal-Organic Frameworks, Chem. Rev. 112 (2012) 673–674, https://doi.org/10.1021/cr300014x.
[2] H.C.J. Zhou, S. Kitagawa, Metal-Organic Frameworks, Chem. Soc. Rev. 43 (2014) 5415–5418, https://doi.org/10.1039/C4CS90059F.
[3] M. Dincă, J.R. Long, Introduction: Porous Framework Chemistry, Chem. Rev. 120 (2020) 8037–8038, https://doi.org/10.1021/acs.chemrev.0c00836.
[4] E. Linnane, S. Haddad, F. Melle, Z. Mei, D. Fairen-Jimenez, The uptake of metal–organic frameworks: a journey into the cell, Chem. Soc. Rev. 51 (2022) 6065–6086, https://doi.org/10.1039/D0CS01414A.
[5] A. Iliescu, J.J. Oppenheim, C. Sun, M. Dincă, Conceptual and Practical Aspects of Metal–Organic Frameworks for Solid–Gas Reactions, Chem. Rev. 123 (2023) 6197–6232, https://doi.org/10.1021/acs.chemrev.2c00537.
[6] N. Stock, S. Biswas, Synthesis of Metal-Organic Frameworks (MOFs): Routes to Various MOF Topologies, Morphologies, and Composites, Chem. Rev. 112 (2012) 933–969, https://doi.org/10.1021/cr200304e.
[7] Y. Sun, H.-C. Zhou, Recent progress in the synthesis of metal-organic frameworks, Sci. Technol. Adv. Mater. 16 (2015) 054202, https://doi.org/10.1088/1468-6996/16/5/054202.
[8] P. Li, F.-F. Cheng, W.-W. Xiong, Q. Zhang, New synthetic strategies to prepare metal–organic frameworks, Inorg. Chem. Front. 5 (2018) 2693–2708, https://doi.org/10.1039/C8QI00543E.
[9] Y. Li, G. Wen, J. Li, Q. Li, H. Zhang, B. Tao, J. Zhang, Synthesis and shaping of metal–organic frameworks: a review, Chem. Commun. 58 (2022) 11488–11506, https://doi.org/10.1039/D2CC04190A.
[10] V.F. Yusf, N. I.Malek, S.K. Kailasa, Review on Metal–Organic Framework Classification, Synthetic Approaches, and Influencing Factors: Applications in Energy, Drug Delivery, and Wastewater Treatment, ACS Omega 7 (2022) 44507–44531, https://doi.org/10.1021/acsomega.2c05310.
[11] T. Azbell, T.A. Pitt, R.T. Jerozal, R.M. Mandel, P.J. Milner, Simplifying the Synthesis of Metal–Organic Frameworks, Acc. Mater. Res. 4 (2023) 867–878, https://doi.org/10.1021/accountsmr.3c00121.
[12] J. Klinowski, F.A. Almeida Paz, P. Silva, J. Rocha, Microwave-Assisted Synthesis of Metal–Organic Frameworks, Dalton Trans. 40 (2011) 321–330, https://doi.org/10.1039/C0DT00708K.
[13] C. Vaitsis, G. Sourkouni, C. Argirusis, Metal Organic Frameworks (MOFs) and ultrasound: A review, Ultrason. Sonochem. 52 (2019) 106–119, https://doi.org/10.1016/j.ultsonch.2018.11.004.
[14] S. Głowniak, B. Szczęśniak, J. Choma, M. Jaroniec, Mechanochemistry: Toward green synthesis of metal–organic frameworks, Mater. Today 46 (2021) 109–124, https://doi.org/10.1016/j.mattod.2021.01.008.
[15] H. Ren, T. Wei, Electrochemical Synthesis Methods of Metal-Organic Frameworks and Their Environmental Analysis Applications: A Review, ChemElectroChem 9 (2022) e202200196, https://doi.org/10.1002/celc.202200196.
[16] E. Parnham, R.E. Morris, Ionothermal Synthesis of Zeolites, Metal–Organic Frameworks, and Inorganic–Organic Hybrids, Acc. Chem. Res. 40 (2007) 1005–1013, https://doi.org/10.1021/ar700025k.
[17] R.E. Morris, Ionothermal synthesis—ionic liquids as functional solvents in the preparation of crystalline materials, Chem. Commun. (2009) 2990–2998, https://doi.org/10.1039/B902611H.
[18] D. Freudenmann, S. Wolf, M. Wolff, C. Feldmann, Ionic Liquids: New Perspectives for Inorganic Synthesis? Angew. Chem. Int. Ed. 50 (2011) 11050–11060, https://doi.org/10.1002/anie.201100904.
[19] B. Zhang, J. Zhang, B. Han, Assembling Metal–Organic Frameworks in Ionic Liquids and Supercritical CO_2, Chem. Asian J. 11 (2016) 2610–2619, https://doi.org/10.1002/asia.201600323.
[20] T.P. Vaid, S. P.Kelley, R.D. Rogers, Structure-directing effects of ionic liquids in the ionothermal synthesis of metal–organic frameworks, IUCrJ 4 (2017) 380–392, https://doi.org/10.1107/S2052252517008326.
[21] A.P. Abbott, G. Capper, D.L. Davies, R.K. Rasheed, V. Tambyrajah, Novel Solvent Properties of Choline Chloride/Urea Mixtures, Chem. Commun. (2003) 70–71, https://doi.org/10.1039/B210714G.
[22] Q. Zhang, K. De Oliveira Vigier, S. Royer, F. Jérôme, Deep Eutectic Solvents: Syntheses, Properties and Applications, Chem. Soc. Rev. 41 (2012) 7108–7146, https://doi.org/10.1039/C2CS35178A.
[23] E.L. Smith, A.P. Abbott, K.S. Ryder, Deep Eutectic Solvents (DESs) and Their Applications, Chem. Rev. 114 (2014) 11060–11082, https://doi.org/10.1021/cr300162p.
[24] B.B. Hansen, S. Spittle, B. Chen, D. Poe, Y. Zhang, J.M. Klein, A. Horton, L. Adhikari, T. Zelovich, B.W. Doherty, B. Gurkan, E.J. Maginn, A. Ragauskas, M. Dadmun, T.A. Zawodzinski, G.A. Baker, M.E. Tuckerman, R.F. Savinell, J. R. Sangoro, Deep Eutectic Solvents: A Review of Fundamentals and Applications, Chem. Rev. 121 (2021) 1232–1285, https://doi.org/10.1021/acs.chemrev.0c00385.
[25] D.O. Abranches, J.A.P. Coutinho, Everything You Wanted to Know about Deep Eutectic Solvents but Were Afraid to Be Told, Annu. Rev. Chem. Biomol. Eng. 14 (2023) 141–163, https://doi.org/10.1146/annurev-chembioeng-101121-085323.
[26] R.A. Maia, B. Louis, S.A. Baudron, Deep eutectic solvents for the preparation and post-synthetic modification of metal- and covalent organic frameworks, CrystEngComm 23 (2021) 5016–5032, https://doi.org/10.1039/D1CE00714A.
[27] R.A. Maia, C.Maxim A.Fluck, B. Louis, S.A. Baudron, Enantiopure natural deep eutectic solvents for metal-organic framework chiral induction, Green Chem. 25 (2023) 9103–9108, https://doi.org/10.1039/D3GC02993J.
[28] R.A. Maia, B. Louis, S.A. Baudron, HKUST-1 MOF in reline deep eutectic solvent: synthesis and phase transformation, Dalton Trans. 50 (2021) 4145–4151, https://doi.org/10.1039/D1DT00377A.
[29] M. Teixeira, R.A. Maia, S. Shanmugam, B. Louis, S.A. Baudron, Impact of urea-based deep eutectic solvents on Mg-MOF-74 morphology and sorption properties, Micropor. Mesopor. Mater. 343 (2022) 112148, https://doi.org/10.1016/j.micromeso.2022.112148.
[30] M. Teixeira, R.A. Maia, L. Karmazin, B. Louis, S.A. Baudron, Ionothermal synthesis of calcium-based metal organic frameworks in a deep eutectic solvent, CrystEngComm 24 (2022) 601–608, https://doi.org/10.1039/D1CE01497H.
[31] M. Teixeira, B. Louis, S.A. Baudron, A blessing and a curse: impact of urea derivatives on the secondary building unit of Ca-MOFs prepared in deep eutectic solvents, Dalton Trans. 54 (2025) 5006–5016, https://doi.org/10.1039/D4DT03254C.
[32] M. Teixeira, S.A. Baudron, Impact of ligand functionalization on the structure of strontium MOFs prepared in a deep eutectic solvent, CrystEngComm 27 (2025) 5421–5430, https://doi.org/10.1039/D5CE00497G.
[33] S.P. Simeonov, C.A.M. Afonso, Basicity and stability of urea deep eutectic mixtures, RSC Adv. 6 (2016) 5485–5490, https://doi.org/10.1039/C5RA24558C.
[34] M. Marchel, H. Cieśliński, G. Boczkaj, Thermal Instability of Choline Chloride-Based Deep Eutectic Solvents and Its Influence on Their Toxicity – Important Limitations of DESs as Sustainable Materials, Ind. Eng. Chem. Res. 61 (2022) 11288–11300, https://doi.org/10.1021/acs.iecr.2c01898.
[35] D. Banerjee, J. B.Parise, Recent Advances in s-Block Metal Carboxylate Networks, Cryst. Growth Des. 11 (2011) 4704–4720, https://doi.org/10.1021/cg2008304.
[36] Y. Zang, S.-Q.Zang L.-K.Li, Recent development on the alkaline earth MOFs (AEMOFs), Coord. Chem. Rev. 440 (2021) 213955, https://doi.org/10.1016/j.ccr.2021.213955.
[37] M.A. Alnaqbi, A. Alzamly, S. Hussein Ahmed, M. Bakiro, J. Kegere, H.L. Nguyen, Chemistry and applications of s-block metal–organic frameworks, J. Mater. Chem. A 9 (2021) 3828–3854, https://doi.org/10.1039/D0TA09678D.
[38] S. Xian, Y. Lin, H. Wang, J. Li, Calcium-Based Metal–Organic Frameworks and Their Potential Applications, Small 17 (2021) 2005165, https://doi.org/10.1002/smll.202005165.
[39] J. Zhang, J.T. Bu, S. Chdengen, T. Wu, S. Zheng, Y. Chen, R.A. Nieto, P. Feng, X. Bu, Urothermal Synthesis of Crystalline Porous Materials, Angew. Chem., Int. Ed. 49 (2010) 8876–8879, https://doi.org/10.1002/anie.201003900.
[40] M. Teixeira, S.A. Baudron, Urothermal synthesis of Metal-Organic Frameworks, CrystEngComm 26 (2024) 5978–5990, https://doi.org/10.1039/D4CE00859F.
[41] G.M. Sheldrick, SHELXT – Integrated space-group and crystal-structure determination, Acta Cryst. A71 (2015) 3–8, https://doi.org/10.1107/S2053273314026370.
[42] G.M. Sheldrick, Crystal structure refinement with SHELXL, Acta Cryst. C71 (2015) 3–8, https://doi.org/10.1107/S2053229614024218.
[43] M86-EXX278V1 APEX4 User Manual, Bruker Corporation, 2021.
[44] A.L. Spek, PLATON SQUEEZE: a tool for the calculation of the disordered solvent contribution to the calculated structure factors, Acta Cryst. C71 (2015) 9–18, https://doi.org/10.1107/S2053229614024929.
[45] CrysAlisPro Software System, Version 1.171.43.70a, Rigaku Oxford Diffraction, 2023.
[46] C.F. Macrae, I. Sovago, S.J. Cottrell, P.T.A. Galek, P. McCabe, E. Pidcock, M. Platings, G.P. Shields, J.S. Stevens, M. Towler, P.A. Wood, Mercury 4.0: from visualization to analysis, design and prediction, J. Appl. Cryst. 53 (2020) 226–235, https://doi.org/10.1107/S1600576719014092.
[47] D.J. Tranchemontagne, J.L. Mendoza-Cortés, M. O'Keeffe, O.M. Yaghi, Secondary building units, nets and bonding in the chemistry of metal–organic frameworks, Chem. Soc. Rev. 38 (2009) 1257–1283, https://doi.org/10.1039/B817735J.
[48] A.E. Platero-Prats, N. Snejko, M. Iglesias, Á. Monge, E. Gutiérrez-Puebla, Insight into Lewis Acid Catalysis with Alkaline-Earth MOFs: The Role of Polyhedral Symmetry Distortions, Chem. Eur. J. 19 (2013) 15572–15582, https://doi.org/10.1002/chem.201302571.
[49] N.R. Kelly, S. Goetz, S.R. Batten, P.E. Kruger, Coordination behaviour and network formation with 4,4′,6,6′-tetracarboxy-2,2′-bipyridine and 4,4′-dicarboxy-2,2′-bipyridineligands with rare and alkaline earth metals, CrystEngComm 10 (2008) 68–78, https://doi.org/10.1039/B711469A.
[50] A. Kobayashi, T. Ohba, E. Saitoh, Y. Suzuki, S.-I. Noro, H.-C. Chang, M. Kato, Flexible Coordination Polymers Composed of Luminescent Ruthenium(II) Metalloligands: Importance of the Position of the Coordination Site in Metalloligands, Inorg. Chem. 53 (2014) 2910–2921, https://doi.org/10.1021/ic402683j.
[51] A. Kobayashi, H. Hara, T. Yonemura, H.-C. Chang, M. Kato, Systematic structural control of multichromic platinum(ii)-diimine complexes ranging from ionic solid to coordination polymer, Dalton Trans 41 (2012) 1878–1888, https://doi.org/10.1039/C1DT11155H.
[52] S. Bhattacharjee, T. Chakraborty, S. Banerjee, A.K. Das, A. Bhaumik, Construction of a series of pH stable Ca-based MOFs, their CO_2 adsorption and catalytic activity, Dalton Trans. 53 (2024) 11120–11132, https://doi.org/10.1039/D4DT01150C.
[53] K.I. Hadjiivanov, D.A. Panayotov, M.Y. Mihaylov, E.Z. Ivanova, K.K. Chakarova, S. M. Andonova, N.L. Drenchev, Power of infrared and Raman spectroscopies to characterize metal organic frameworks and investigate their interaction with guest molecules, Chem. Rev. 121 (2021) 1286–1424. https://pubs.acs.org/doi/10.1021/acs.chemrev.0c00487.
[54] D.S. Raja, J.-H. Luo, C.-T. Yeh, Y.-C. Jiang, K.-F. Hsu, C.-H. Lin, Novel alkali and alkaline earth metal coordination polymers based on 1,4-naphthalenedicarboxylic acid: synthesis, structural characterization and properties, CrystEngComm 16 (2014) 1985–1994, https://doi.org/10.1039/C3CE42208A.

[55] W.J. Zhu, Z.J. Qin, Y. Bai, D.B. Dang, Geminal dicationic ionothermal synthesis of one three-dimensional luminescent strontium(II) coordination polymer based on 1,4-naphthalenedicarboxylate acid, Russ. J. Coord. Chem. 44 (2018) 425–431, https://doi.org/10.1134/S1070328418070096.
[56] D. Kojima, T. Sanada, N. Wada, K. Kojima, Synthesis, structure, and fluorescence properties of a calcium-based metal–organic framework, RSC Adv. 8 (2018) 31588, https://doi.org/10.1039/C8RA06043F.
[57] S.-L. Yao, S.J. Liu, X.-M Tian, T.-F. Zheng, C. Cao, C.-Y. Niu, y.Q. Chen, J.-L. Chen, H. Huang, H.-R. Xen, A Zn^{II}-based metal−organic framework with a rare tcj topology as a turn-on fluorescent sensor for acetylacetone, Inorg. Chem. 58 (2019) 3578–3581, https://doi.org/10.1021/acs.inorgchem.8b03316.
[58] X.-G. Guo, W.-B. Yang, X.-Y. Wu, Q.-K. Zhang, L. Lin, R. Yu, C.-Z. Lu, Stoichiometry, temperature, solvent, metal-directed syntheses of metal–organic frameworks based on flexible V-shaped methylenebis(3,5-dimethylpyrazole) and various aromatic dicarboxylate acids, CrystEngComm 15 (2013) 3654–3663, https://doi.org/10.1039/C3CE00048F.
[59] M. D. Allendorf, C. A. Bauer, R. K. Bhakta, R. J. T. Houk, Luminescent metal-organic frameworks; Chem. Soc. Rev. 38 (1330) 1330-1352. https://doi.org/10.1039/B802352M.